

HINGED TRUCHET TILING FRACTALS

H. A. VERRILL H.A.VERRILL@WARWICK.AC.UK

ABSTRACT

This article describes a new method of producing space filling fractal curves based on a hinged tiling procedure. The fractals produced can be generated by a simple L-system. The construction as a hinged tiling has the advantage of automatically implying that the fractiles produced tessellate, and that the Heighway fractal dragon curve, and all the other curves constructed, do not cross themselves. This also gives a new limiting procedure to apply to certain Truchet tilings. I include the computation of the fractal dimension of one of the curves, and describe an algorithm for computing the sim value of the fractal boundary of these curves. The curves considered have previously been described by [Tab14], but the hinged tiling approach is new, as is the algorithm for computing the sim value.

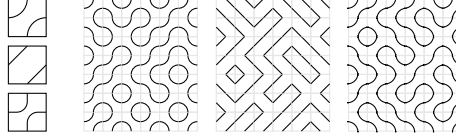


FIGURE 1. Some Truchet tiles and examples of their tilings

1. INTRODUCTION

Space filling curves are a concept introduced by Peano in 1890 [Pea90], simplified by the Hilbert curve in 1891 [Hil91]. Since then many other space filling curves have been found see e.g., [Sag94]. There are many ways to modify Hilbert's original construction e.g., [Ozk21], and many other constructions exist. Space filling curves have applications in computer science e.g. [Bad13], [Böh20].

In this article, I start with a Truchet tiling, and iteratively produce a related tiling of the same form, in a continuous way. By taking the limit, a space filling curve is achieved.

A *Truchet tiling* is a set of identical square tiles arranged together in different rotations. Named after Truchet who wrote about them in 1704, they were popularised more recently by [Smi87], especially the top left tile Figure 1. These tilings are widely used in generative art work and graphic design, for example [Kra11], [Car18], and also have been applied in computer graphics [Bro08].

In this article I restrict to the tiles of Figure 1. These are deformations of each other, and have the same symmetry groups. There is not a great deal of difference in the mathematics of the curves produced. I will switch between tiles, but everything I say about one case applies to the others.

Hinged tilings are popular and well known in recreational mathematics [Fre02], and have applications in origami [Lan18], [Bar92]. We use the simplest hinged tiling, that of squares, Figure 2.

2. HINGED TRUCHET CURVE GENERATION

Figure 2 shows how a hinged tiling application to a Truchet tiling leads to another Truchet tiling. After the hinging process is applied to open the tiling to maximum extent (third picture

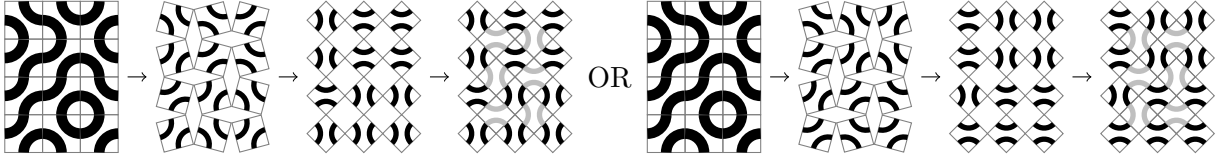


FIGURE 2. Hinged Truchet tiling, two possible directions

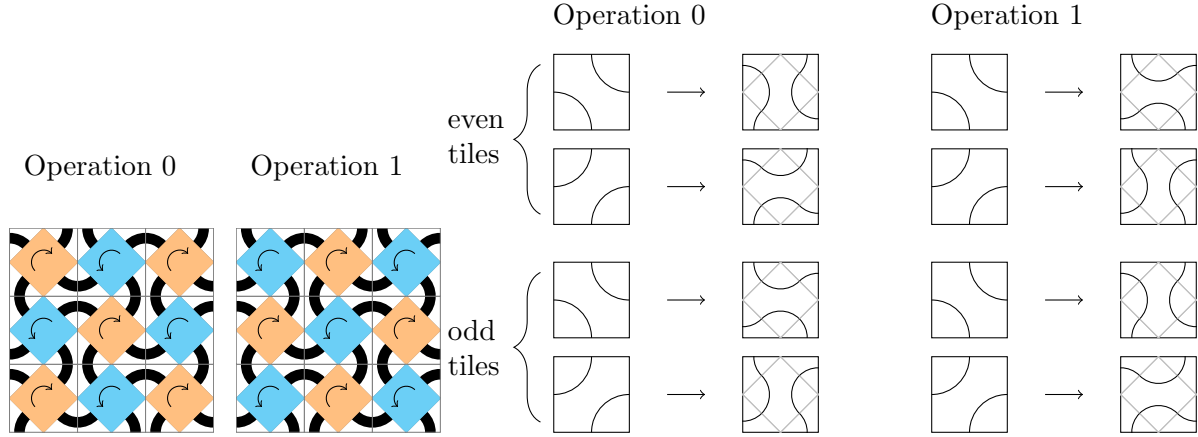


FIGURE 3. How the new tiles are added in hinged tiling, for either of the two operations, and an alternative way to see the transformations as a replacement rule. Even and odd refer to the grid position of the tile.

in sequences), there is only one way in which the tiling can be completed with the same kind of tiles to preserve the connected components of the tiling, as shown. The added tiles are coloured grey instead of black to help distinguish them. There are two possible ways to hinge the tiling, depending on the direction of rotation. Alternate squares rotate in opposite directions, and remain connected at appropriate corners. In a traditional hinged tiling, the squares would remain the same size, but in this version, each square tile is scaled down so that the vertices which meet adjacent tiles move along the original tile. Figure 3 left shows how the added tiles are inserted, in either case of the direction of turning. The tiles are coloured according to the direction of rotation. These two cases are determined by the convention that the tiles are labeled alternately odd or even, which can be considered as the parity of the sum of the coordinates when tiles are indexed by integer coordinates. Operation 0 is where even tiles rotate clockwise, odd tiles anti-clockwise; operation 1 is the reverse. After the operation is applied, I use the convention that all the old tiles are now even, and all the added tiles are now odd. It is important to have some consistent convention, in order to apply the operations repeatedly.

This procedure can also be viewed as a replacement of each tile by smaller tiles as in Figure 3 right. This can be compared with the replacement rules for the Hilbert space filling curve, explored in detail in [Ozk21], however, in this case the tile is divided into parts which do not fit as single whole units into the original tile. Possibly there are other dissections possible for tile replacements. The replacement rule in Figure 3 only has four cases because the tiles have 180° rotational symmetry. A longer list of rules would be needed in less symmetric cases. The tiles can be rotated in a continuous fashion, and the added tiles can be incorporated as the original tiles are rotated, rather than added at the end, so the procedure can be considered as a continuous transformation rather than a discrete operation. This shows that the number of components of a Truchet tiling path configuration does not change with this operation. A program illustrating this in motion can be found at [Ver21].

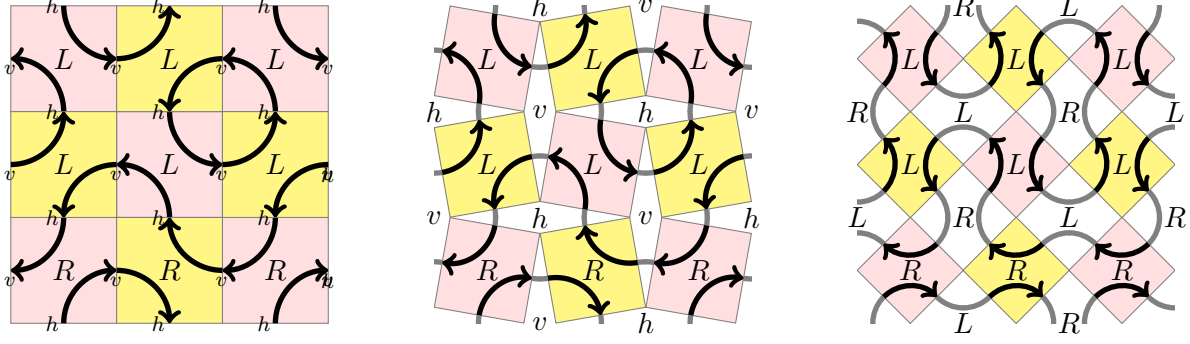


FIGURE 4. Sequence showing transformation of paths, directions of flow, and labeling of paths on a Truchet tiling. This shows operation 0, with $v \rightarrow L$ and $h \rightarrow R$.

operation 0		operation 1	
L	\rightarrow L	L	\rightarrow L
R	\rightarrow R	R	\rightarrow R
h	\rightarrow hLv	h	\rightarrow hRv
v	\rightarrow hRv	v	\rightarrow hLv

TABLE 1. L-system description of hinged tiling operations.

3. L-SYSTEMS

The effect of the procedure described on the curves can be described as an L-system. An L-system is a method of describing growth processes developed by Lindenmayer [Lin68]. In our case, words describe directions for drawing a path. A replacement rule on the letters of the word gives instructions to generate the next step in the procedure.

Paths on Truchet tilings of the form we are interested in can be given consistent “in” and “out” directions as shown by the arrows in the example in Figure 4. The tiles’ orientation determine whether the path curves left or right into the next square. Thus each path can be described by a sequence such as $RvLhRvLhLvR$ as seen in the figure, and more generally, a path is given by a sequence $XvXhXvXh\dots$ where X is either R or L . The R label is used when the path is turning right, and the L when turning left. In the figure, for less clutter and more clarity, the letters R and L only appear once per tile, which is possible since both paths in any tile turn in the same direction. The label v is used for crossing a vertical line, and h for crossing a horizontal line. In the figure, the dark squares are considered even, and this is an application of operation 0. As the operation is applied, the new tiles added in the spaces labeled v or h are replaced with tiles with paths turning either left or right respectively. When the new tiles appear, there will be new “horizontal” and “vertical” lines to cross. The tiling is now rotated by 45° . However, we are using the convention that all the original tiles remain or become even, and so this determines which of the diagonal lines are labeled h or v , because the direction of flow is always into an even tile from a h line, and into an odd tile from a v line. So in the rightmost diagram in Figure 4 the NW–SE lines should be labeled h and the NE–SW lines should be labeled v .

The rules for the procedures described in this paper are as in Table 1

3.1. Notation. For the remainder of this paper, I will denote paths by a sequence of L s and R s, e.g., $LRRRLL$, and combinations of operations 0 and 1 by a sequence of 0s and 1s. Thus for example $00101LLR$ means start with a path defined by the directions LLR , then apply the operations in the order from *left to right*, i.e., operation 0, then operation 0, then operation 1 and so on.

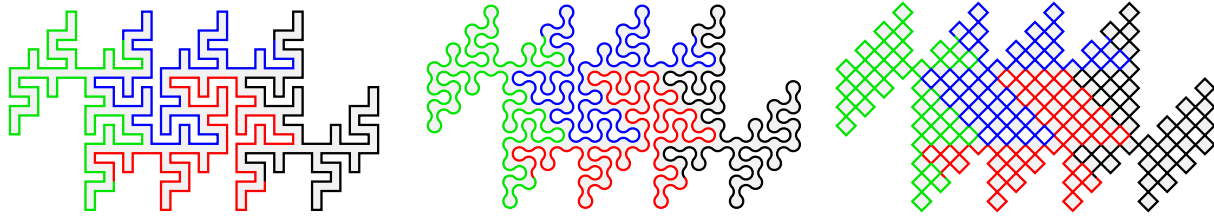


FIGURE 5. Comparison of 0100010RRRR for different tile designs.

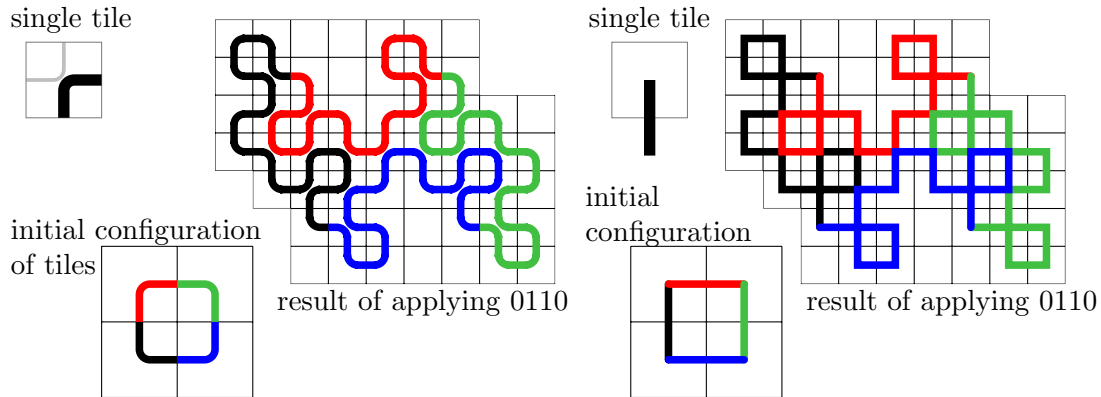


FIGURE 6. Comparison of tile in the hinged tile construction (left), and a replacement tile comparable to the usual Heighway dragon construction (right). The sequence of operations 0110 has been applied to the initial square arrangement of line segments.

4. COMPARISON WITH HEIGHWAY'S FRACTAL DRAGON

In [Tab14] the fractal Heighway dragon curve is described as being obtained from an L system equivalent to that in Table 1, applying only operation 0 repeatedly. The rules described in [Edg08] are interpreted as drawing a line, then making a turn, and so on. For the hinged tiling method, we can put different designs on our tiles, which for the finite cases may look somewhat different, but in the limit will all end up being the same. Figure 1 shows some different possible tiles, and Figure 5 compares the result of applying the operation 0100010 to the initial configuration $LLLL$. To compare with the construction of the Heighway dragon given in [Edg08,], we slightly alter our curves as in Figure 6. All this means is that for the usual construction, the lines, if drawn on tiles, are considered going from centre of tile to centre of tile, whereas in the original Truchet tiling construction the tiles go from edge to edge. In the Truchet tiling construction we may have many components, producing many curves simultaneously, whereas in the standard construction we just start with one component. So in Figure 6 I have coloured the components in different colours, including leaving some parts of tiles only having half the design shown.

By construction, the Truchet tilings we start with are always non-self intersecting, and tessellate. Each step of the iteration always produces another Truchet tiling. So results about non-self intersection and tessellation given in [Edg08] and [Tab14] are now obtained automatically.

5. FRACTAL DIMENSION

5.1. Space filling. The curves described here are space filling: take a single tile with just two components. Consider the Truchet tiling to take place on the surface of a torus with initially only one square. On the torus the configuration now consists of a closed ring of two components, and

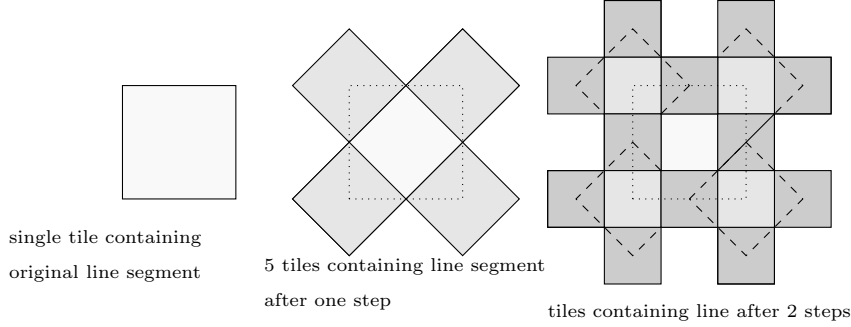


FIGURE 7. Argument that after infinite application of 0 and 1, the resulting curve is contained in a finite region. First two applications of process shown.

no end points. Now apply any infinite sequence of the operations 0 and 1. At each step, a finer grid of tiles is covered. In the limit the whole torus is covered, with points of the curve arbitrarily close to any point of the torus. Now unroll our torus to the plane. We get a tessellation of the tiles covering the plane. We have to rule out the possibility of individual tiles not being contained in a finite region. This follows by considering the iteration step in the hinged tiling. For any single line segment, the iteration step takes the curve to a new curve completely contained in the same square. However, each square is not contained in the previous square, so after one step, a curve is contained in the original square, and in two adjacent squares, but the adjacent squares, and the scaled original square have side length only $\sqrt{2}$ the original side length. So, taking the initial squares to have unit length, after two steps, the curve is contained in a square of side length 1 and square of side length $\sqrt{2}$. The new points added to the curve are at most $\sqrt{2}$ from the initial curve. At successive steps we can get points further away by increments of $\sqrt{2}$. So the maximum total possible distance of any point in the limit curve is $\sum 2^{-n/2} = 2 - \sqrt{2} < 1$. This is illustrated in Figure 7. This means that the whole of the initial square must be covered by fractiles (using the terminology of [Edg08] for tiles with (possibly) fractal boundary) derived from curves at most in the adjacent squares, so will have at most 9 of these curves covering a square. Hence since there are only a finite number of curves covering a square, and since they are images of each other, they must cover a non empty open set and thus be space filling. Since these are space filling curves, they have fractal dimension 2 [Edg08].

5.2. Fractal dimension of boundary. It is known that the fractal dimension of the boundary of the fractal dragon curve is approximately 1.52 [Edg08, p 195]. Following the same procedure as Edgar, we now compute the fractal dimension of another curve in our family.

Suppose we apply an infinite sequence of operations, denoted by $B = b_0, b_1, \dots$, where $b_i \in \{0, 1\}$ and $b_i = 0$ and $b_i = 1$ indicate application of operations 0 and 1 respectively. If B is repeating, then we will obtain a curve with a self similar nature. If there is a finite string before the repeating form, ie., $B = ACCCCCC \dots$, then the resulting curve has the form of a finite union of curves obtained from C , and so the fractal dimension is that of C . In the case of non-repeating B , then it's not clear how to compute the fractal dimension of the boundary. Now I will describe a few of the repeating cases.

5.3. Case 0^∞ and 1^∞ . As previously mentioned, this is the case of Heigway's Fractal dragon curve. An example is shown in Figure 19. In [Edg08, p 194,195] it is shown that the fractal dimension of the boundary, (Hausdorff and packing and sim dimensions) is approximately 1.52.

Since we will use the argument from [Edg08] for several other cases, I will reproduce the argument for the computation of the fractal dimension of the boundary here, but using our notation. Figure 8 shows the first few applications of operation 0 to an edge which I label R , and which I consider to

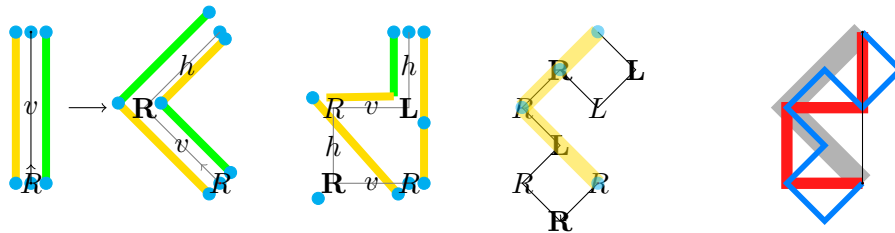


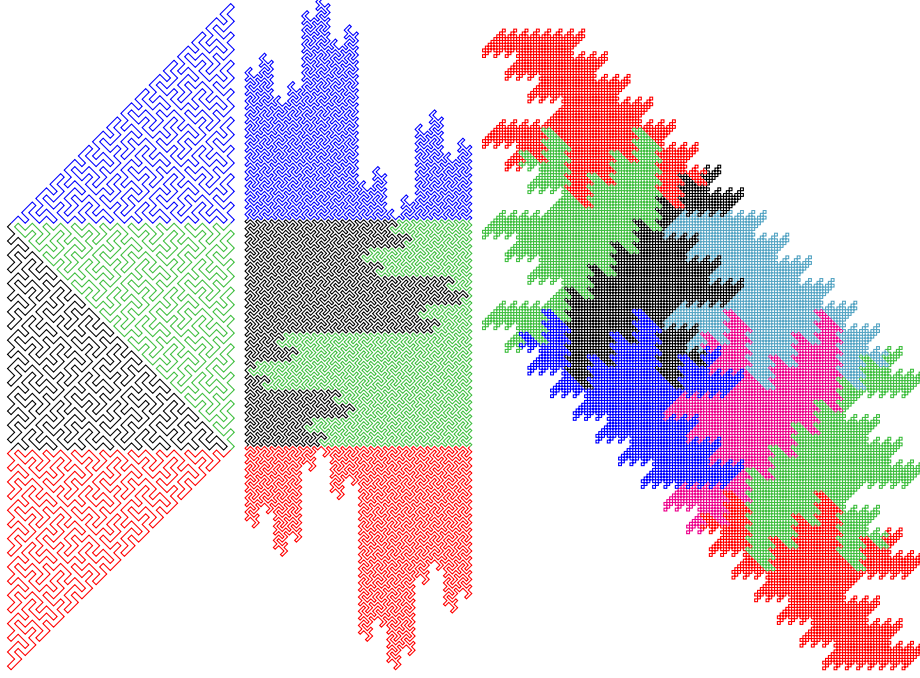
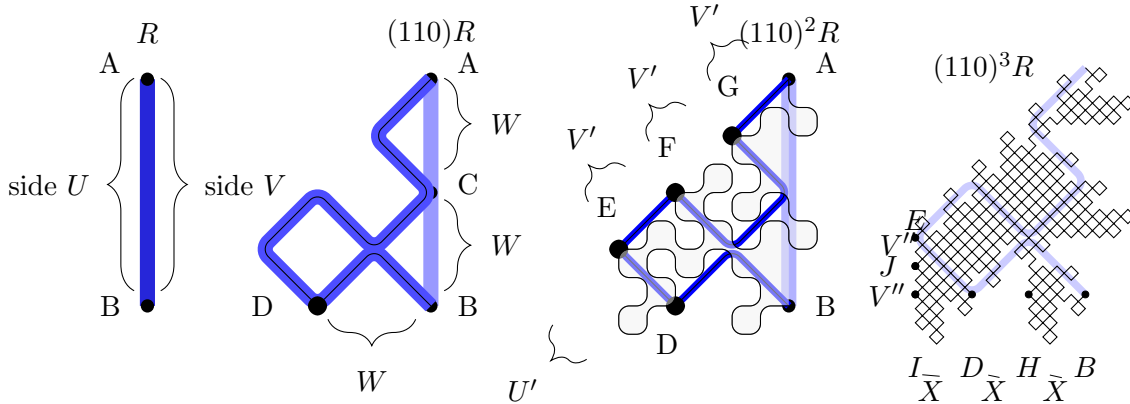
FIGURE 8. First steps in construction of $0^\infty L$. Operation 0 applied each time: $h \rightarrow hLv$, $v \rightarrow hRv$.

start from the top. I label this line v , although it probably should be labeled h , since it crosses a horizontal line, so the images in this figure might be better rotated by 90° .

Remember that our paths are notated in the form $XvXhXvXhX\ldots$ with $X = L$ or R . Only the L or R are evident in the motion, the v and h determine the transformation. From Figure 6, the lines we are now using following Edgar’s construction, have L or R at the end points, and h or v in the middle, rather than the other way round. In this figure, I label the new L and R which appear from the h and v , in bold to help see how they are introduced. The h and v on the segments helps show how although the lines look the same at any stage, the h and v mean they will transform in different ways. However, traveling in the opposite direction along a line, R and L are reversed, so the left and right sides of the path reverse, that is, if we apply an operation B consisting of 0 and 1s to L and to R , then they will have the same boundaries, but on opposite sides. In [Edg08], the left side of $0^\infty L$ is called U and the right side V . I colour these yellow and green respectively in the diagram. I also label points that are in the boundary by blue dots. The yellow and green lines are not in the boundary, but they are getting closer and closer to the boundary; the boundaries on either side are the limits of theses lines. The yellow lines converge to scaled copies of U and the green converge to scaled copies of V .

The right most image shows the first four stages superimposed to help show their relationship to each other. The yellow lines indicate the left hand boundary and the green the right hand boundary of v lines, reverse for h lines. Blue dots corresponding to points lying on the boundary of the limit shape. The two sides of the line should join at the dots at either end, but are shown separated for clarity. Our aim is to find self similarity, and we are going to express the yellow boundary in terms of itself. This means that once we have a yellow component of the left side which is smaller than the initial component, we don't have to decompose further, so in the third and fourth figure, although we could decompose the yellow line from the second step further, we don't bother. The yellow horizontal line in the third image is not in the boundary, because its end points are not both in the boundary. The lower vertical yellow line in this image is in the boundary, but this comes from the limiting boundary of the tile to the right of the tile in question. At this step, the green side, which converges to V , is seen to be two half size copies of the yellow side U , so we don't need to analyse further the right side. In the fourth image, the upper diagonal yellow line is a boundary line coming from boundaries from the adjacent tiles. In this image, since we have already decomposed the right side, the colours yellow and green only refer to the left side boundary. From the fourth picture, we now have $U = \frac{\sqrt{2}}{2}U + \frac{\sqrt{2}}{4}U + \frac{\sqrt{2}}{4}U$. This is the self similarity decomposition which leads to the computation of the fractal dimension of the boundary of the fractal dragon in [Edg08].

5.4. **Case 010101010....** In this case, a single line ends up converging to a triangle shape, and a union of four lines in a ring converges to a closed curve with an overall parallelogram shape. The limit of the boundaries is a straight line, and so the boundary is not fractal. Examples of approximations are shown in Figure 9 left.

FIGURE 9. The closed curves $(01)^5 LLLL$, $(0011)^3 LLLL$, and $(001)^3 RLLLRLLL$.FIGURE 10. Self similarity comparison of $(001)^\infty R$.

5.5. **Case** $0011001100110011\dots$. In this case, as in the case of $01010101010\dots$, a union of two of the fractiles forms a square. However, whilst the boundary is self similar and not straight, it appears that the box counting dimension is 1, because the boundary is mostly composed of straight lines. This is illustrated in Figure 9 centre. This case appears to be the same as one of the examples given in [Tab14, Figure 7].

5.6. **Case** $(001)^\infty$ **and** $(110)^\infty$. In this case, the fractal dimension of the boundary turns out to be approximately 1.4128. We follow [Edg08, 194–195] in making this computation. We consider this curve as being produced by repeated application of the operation 001 to the straight line segment corresponding to Lh . The first few applications of this operation are shown in Figure 10.

Consider Figure 10. Following Edgar, the left side of $(001)^\infty R$ is labeled U and the right side V . Considering $(001)L$, we see that V consists of two identical pieces W , and that the boundary

between points B and D also has form W . By considering $(001)^2L$, we see that the edge DE is a scaled copy of U , namely $U' = 2^{-3/2}U$, and that the edges EF, FG, GA are all scaled copies of the edge V , namely $V' = 2^{-3/2}V$. This results in $U = V' + V' + V' + U' + W$. Now considering $(001)^4L$ we see (also by comparing with the adjacent tiles, as in Figure 9 right), that the edges W have a rotational symmetry about their mid points. So we now write W as the union of two identical pieces X , so $W = X + X$. Also we now see that the component of the edge from I to E is the same as two scaled copies of V , namely $V'' = 2^{-3}V$. So we have $U' = X + V'' + V''$, i.e., $2^{-3/2}U = X + 2^{-3}V + 2^{-3}V$, or equivalently, $U = 2^{3/2}X + 2^{-3/2}V + 2^{-3/2}V$. We also have $V = X + X + X + X$, so this gives $U = 2^{3/2}X + 2^{-3/2}(X + X + X + X + X + X)$. Now notice that the X edge, as below the HB line in is identical, up to a scale factor of $2^{3/2}$, to the edge BF in lower left of this line, which I will call BF^- . From Figure 10, we have $BF^- = V' + U' + W$, so together with $BF^- = 2^{3/2}X$, we have $2^{3/2}X = V' + U' + W = 2^{-3/2}V + V'' + V'' + X + X + X = 2^{-3/2}(X + X + X + X) + 2^{-3}(V + V) + X + X + X = 2^{-3/2}(X + X + X + X) + 2^{-3}(X + X + X + X + X + X + X + X) + X + X + X$. Now we have an expression for X in terms of copies of itself, namely

$$X = 2^{-3}(X + X + X + X) + 2^{-9/2}(X + X + X + X + X + X + X + X) + 2^{-3/2}(X + X + X).$$

For brevity, I rewrite this formula as

$$(1) \quad X = 2^{-3}X^{\oplus 4} + 2^{-9/2}X^{\oplus 8} + 2^{-3/2}X^{\oplus 3}$$

Since U and V are both unions of a finite number of scaled copies of X , all the edges have the same fractal dimension as X . To find this dimension, (following [Edg08, Theorem 6.5.4., p193]) we now need to find s , the sim value, such that

$$4 \times (2^{-3})^s + 8 \times (2^{-9/2})^s + 3 \times (2^{-3/2})^s = 1.$$

This implies $2^{-3s/2}$ is a root of

$$8\lambda^3 + 4\lambda^2 + 3\lambda - 1 = 0,$$

which has only one real root, $\lambda \approx 0.23017$, so the fractal dimension is $s = \frac{2}{3} \log_2(1/\lambda) \approx 1.4128$.

Figure 11 illustrates sets corresponding to the relationship in Equation 1. In this figure, the blue line, which can be described as $F = LLLR$ is given in blue. The gray line is $(001)F$, and the black line is $(001)^2F$. The set X is equal to the boundary of the upper side of $(001)^\infty F$. To decompose X , we look for copies of F in the partial iterations $(001)^n X$.

The red and orange lines are the three copies of $2^{-3/2}F$. The red lines are contained in $(001)F$, and the orange is in a neighbour of $(001)F$. The 4 copies of $2^{-3}F$ are given by the green and cyan lines, which are in $(001)^2F$ and a neighbouring tile respectively, and the violet and brown lines are the 8 copies of $2^{-9/2}F$.

5.7. Moran open set condition. As in [Edg08], to complete the proof that this is the fractal dimension, we need to show that the Moran open set condition [Edg08, p 191] is satisfied. The open set condition is that there is an open set U such that for the iterated system f_1, f_2, \dots, f_n , the $f_i(U)$ are disjoint and contained in U . For us, the f_i are the 15 functions translating the blue region in Figure 11, third figure, to the coloured regions round the lower boundary of this shape in Figure 11 fourth figure. A suitable set U is found to be that given in Figure 12. The left image shows the set S of lines corresponding to the directions $LLRRRLRLRLR$. The right picture is $(001)^2S$. Our open set U is the interior of $(001)^\infty S$, which will look similar to the right figure.

I will replace S by a slightly smaller set, where the far left yellow region is left out, since then it is easier to see that the images $f_i(U)$ are all disjoint. Figure 13 shows the images of (the slightly smaller) U under the action of the f_i illustrating that these regions are all disjoint, and are all contained in U . In this figure, the pink region is the set U , shown in Figure 12, but all in one colour in this figure. On top of the set U , all the images $f_i(U)$ are shown, with the same colours used as in the fourth image in Figure 11.

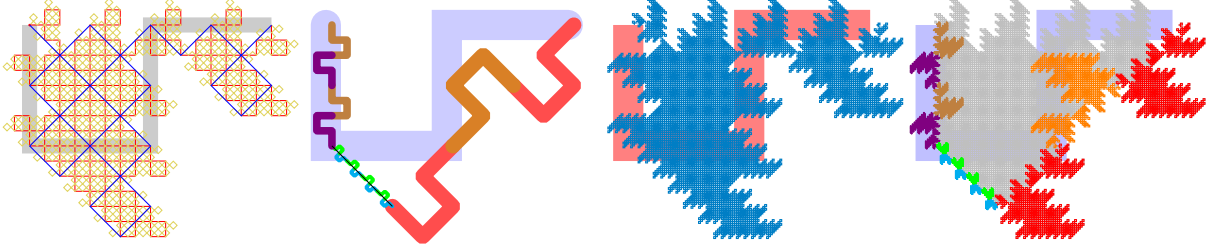


FIGURE 11. A self similar decomposition of X for computing the fractal dimension of the boundary of $(001)^\infty L$. From left to right, the first image shows superimposed $(001)^n LLLR$ for $n = 0, \dots, 3$, the second picks out various copies of $LLLR$ in the boundary of $(001)^n LLLR$. The third shows $(001)^4 LLLR$, the lower boundary of which is X . The fourth shows how applying $(001)^\infty$ (4 rather than ∞ for the purposes of the drawing) to the components in the second image results in the lower boundary in the third image, showing the self similarity of X .

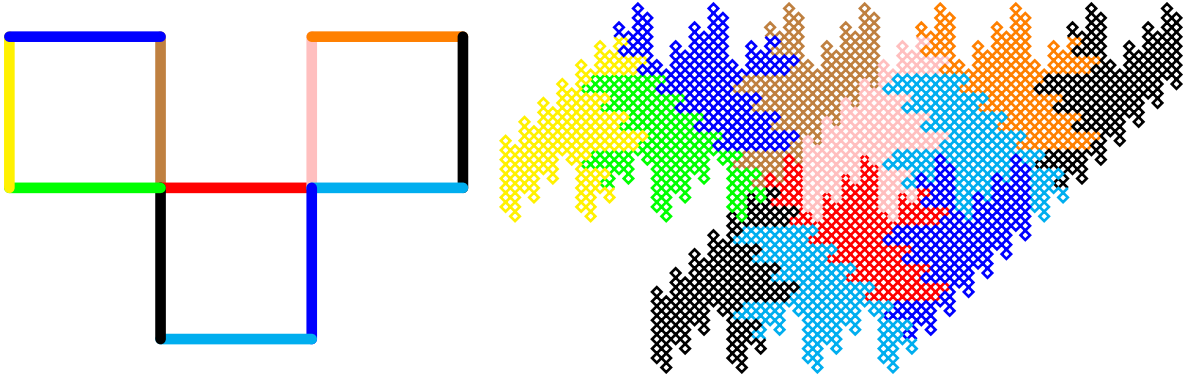


FIGURE 12. $S = LLLRRRLRRLRR$ and $(001)^3 S$. The interior of the limit $(001)^\infty S$ is used as a Moran open set.

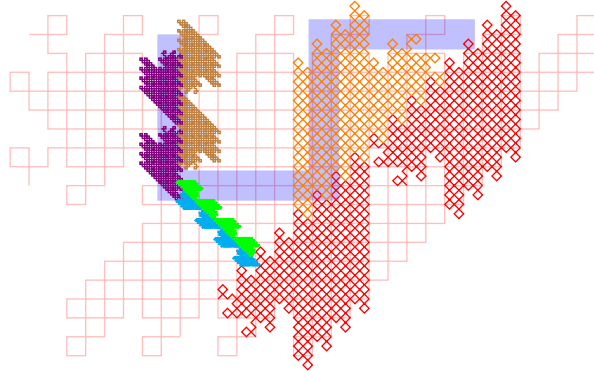
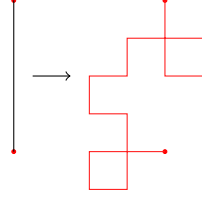
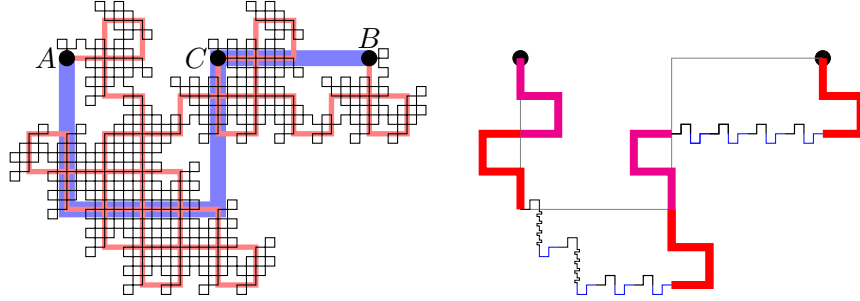


FIGURE 13. Illustration that the Moran open set condition is satisfied.

5.8. **Case $(0001)^\infty$.** To visualise this case, see Figure 21, which shows $(0001)^3 L$. Figure 20 shows $(0001)^2$ applied to a configuration of lines corresponding to $RLRRLRRRLRRRLR$. The action of (0001) on one edge is shown in Figure 14. This is two copies of 001 applied to the edge, since the first application of operation 0 results in two edges, then 001 is applied to both. So we will use the same strategy as for $(001)^\infty$. We take the shape $LLLR$ again. Several applications of 0001 to this

FIGURE 14. The line L and its image $(0001)L$.FIGURE 15. $(0001)^n LLLR$ for $n = 0, 1, 2$. The lower boundary from A to B is Y .

configuration are shown in Figure 15, left. Note that the upper side of this configuration is given by four scaled copies of the lower side. So to compute the fractal dimension of the boundary, we just need to work this out for the lower side, that is, whatever appears on the lower side between A and B . I will call this boundary Y . In Figure 15, right copies of LLL are shown round the boundary of LLL . Note that care must be taken in that the image of the point C in these copies is not a boundary point, but images of A and B are. In this figure, the lines lie on three different grids, corresponding to the blue, red, or black lines. Imagine in each grid of lines, an edge is coloured or left blank. A vertex (points where grid lines intersect) is in the boundary of Y if exactly two of the four edges are coloured. From this figure, we see that

$$Y = \frac{1}{4}Y^{\oplus 5} + \frac{1}{16}Y^{\oplus 16} + \frac{1}{64}Y^{\oplus 16}.$$

So the sim-value is $s \approx 1.4476$, where $\lambda = 2^{-2s}$ is a root of

$$(2) \quad 16\lambda^3 + 16\lambda^2 + 5\lambda = 1.$$

6. ALGORITHM TO FIND SIM VALUE

We have found the sim value for the $(001)^\infty$ and $(0001)^\infty$ in an ad hoc way. Now we present a more systematic method to find the sim value for the case B^∞ for any finite sequence B of 0s and 1s representing a sequence of our operations.

First consider a grid of the initial lines. Remember that in a Truchet tiling path, there is a consistent direction of travel along paths, which we denoted by arrows in Figure 4. In Figure 16, the background grid is drawn in black lines. The paths on the tiles as described in Figure 5 right, are drawn in yellow and green lines, as we did in Figure 8. We will apply the same operation B to the whole grid. A sequence such as $LhRvL\dots$ tells us which lines to follow on a grid path, and if we just take single lines, then the result will be tessellating tiles. The transformation of the path depends on whether the starting tile is odd or even, and whether the grid line crossed is horizontal or vertical. So I put pink circles on the even tiles to distinguish them. In the limit of applying B^∞ , the yellow side of the line will become a boundary U and the green side a boundary V . The orientation of these lines is determined by whether or not they start at an even or odd square.

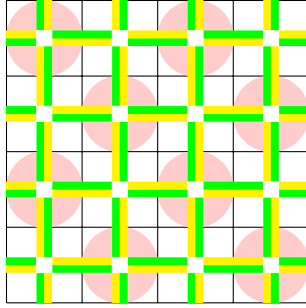


FIGURE 16. Colouring of line segments according to eventual boundary of limiting space filling curves.

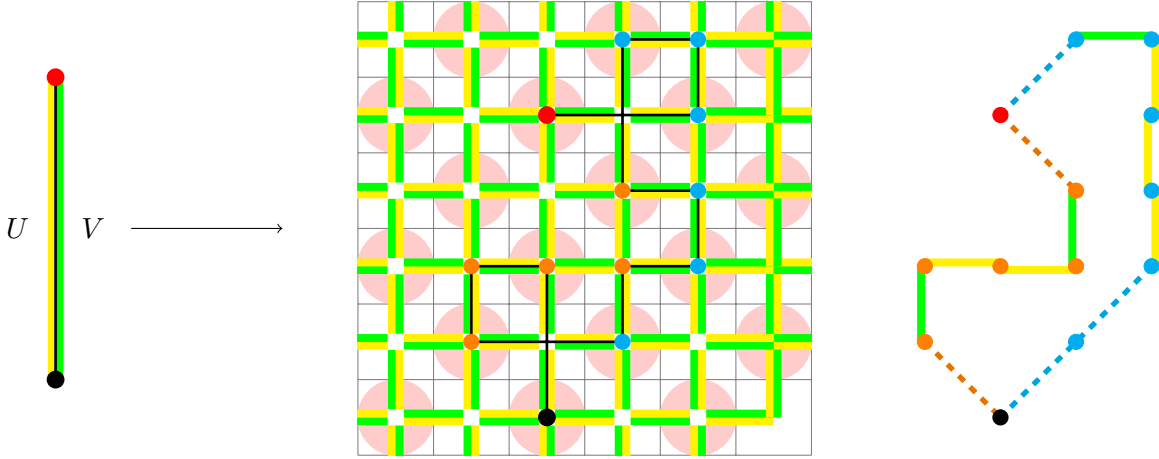
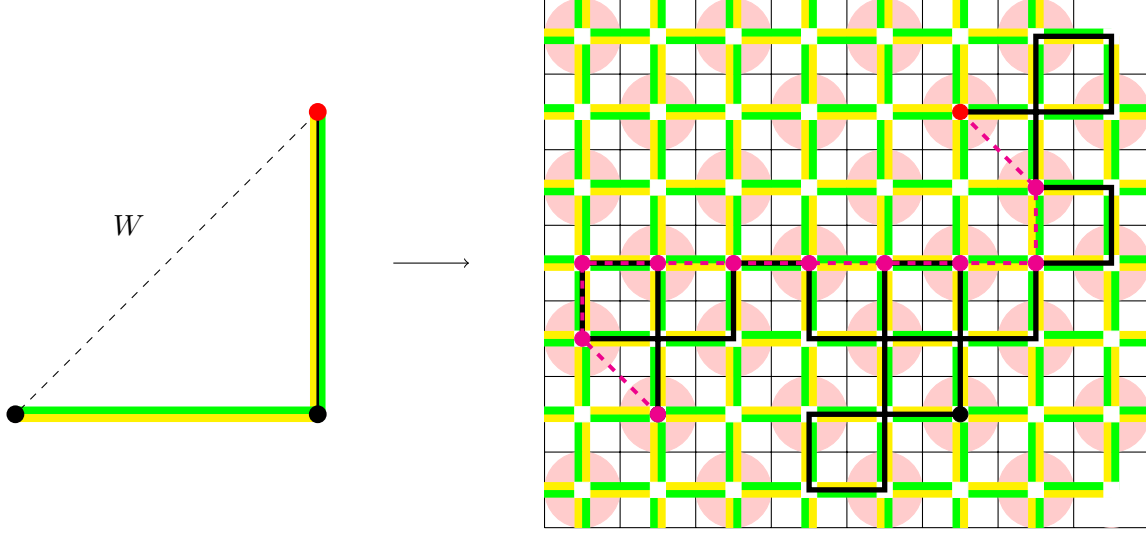


FIGURE 17. $L \rightarrow 0001L$

Now consider the action of our sequence of operations B on a single line segment, for example $B = 0001$. We draw the result of $0001L$ in Figure 17. U indicates the limit of the left side of a line L going down from an even square, and V is the right side, marked in yellow and green respectively. On this figure, the red and black dots indicate the starting and ending points of the line respectively. These are both boundary points of U and V . Of the other vertices, those which are in the boundary of U are coloured with an orange dot, and those which are in the boundary of V are coloured with a blue dot.

Our goal is to write U and V in terms of smaller copies of themselves. In Figure 17 we see we also need a diagonal component, given by the limit of the concatenation of the U and V at right angles to each other. We call this diagonal component W , and how it transforms under 0001 is shown in Figure 17. Let U', V', W' be U, V, W scaled by a factor of $\frac{1}{4}$ respectively. Figure 17 right follows round the path in the middle grid to show how U and V are given in terms of U', V', W' . The situation for W is shown in Figure 18. The magenta points are in the boundary of W , and following the dashed line path through them we can read off $W = W' + U' + 6V' + W'$. From these

FIGURE 18. Image of $W = LR$ under 0001

figures we have the system of equations:

$$U = 2U' + 2V' + 2W'$$

$$V = 3U' + V' + 3W'$$

$$W = 6U' + 2V' + 2W'$$

We can rewrite this as a matrix equation

$$(3) \quad \mathbf{U} = M\mathbf{U}' \text{ where } M = \begin{pmatrix} 2 & 2 & 2 \\ 3 & 1 & 3 \\ 6 & 2 & 2 \end{pmatrix}, \mathbf{U} = (U, V, W)^T.$$

Here $\mathbf{U}' = (U', V', W') = (sU, sV, sW)$ where the scale factor is $s = \frac{1}{4}$. In general, if B has length n , the factor s will be $2^{-n/2}$. To find the fractal dimension of U and V , we want to find the sim value of some shape X composed of a union of U, V, W . Suppose we have $X = \alpha U + \beta V + \gamma W$, which we write as

$$X = A\mathbf{U},$$

where $A = (\alpha, \beta, \gamma)$. In order to write X in terms of $X', X'',$ and X''' (which are equal to sX, s^2X, s^3X), we write everything in terms of X''' . By repeated application of M , we see that

$$X = AM^3\mathbf{U}'''$$

$$X' = AM^2\mathbf{U}'''$$

$$X'' = AM\mathbf{U}'''$$

$$X''' = A\mathbf{U}'''$$

Writing $X = (a, b, c)(X', X'', X''')$ for some non negative integers a, b, c implies that

$$A(M^3 - aM^2 - bM - cI) = 0.$$

For this to be possible, we must find non negative integers a, b, c with $\det(M^3 - aM^2 - bM - cI) = 0$. To do this, it is sufficient to find the characteristic polynomial c_M of the matrix M . Provided all but the leading term have non positive coefficients, our a, b, c are provided, and we can just take

$X = U$. In this example, it turns out that $c_M(x) = x^3 - 5x^2 - 16x - 16$. These give the coefficients in Equation 2, which determine the sim value as previously computed.

To summarize, the outline of the algorithm to compute the sim value of the boundary of $B^\infty L$ (where L is an initial line) for some finite binary string B of length one is as follows:

- (1) Draw BU, BV and BW , as in examples in Figures 17 and 18.
- (2) Find a matrix M to express U, V, W in terms of sU, sV, sW for $s = 2^{-n/2}$.
- (3) If possible, find non negative integers not all zero α, β, γ and non negative not all zero a, b, c such that if $c_M(x) = x^3 - ax^2 - bx - c$ then $(\alpha, \beta, \gamma)c_M(M) = 0$. If this is possible, we can proceed to the next step.
- (4) Let λ be a real root of c_M . Then the sim value of $B^\infty L$ is

$$s = \frac{-2 \log(\lambda)}{n \log(2)}.$$

7. FUTURE WORK

It remains to show that the algorithm for finding the sim value gives the fractal dimension, for which we need an algorithm for finding a Moran open set. We also need to automate the process of computing the matrix M , by writing a program for computing the boundaries of BL and BLR , which was done by hand in Figures 17 and 18. Then it would be possible to investigate the possible values and the upper bound on the fractal dimensions obtained from this process. Many of the diagrams for this paper were produced by a JavaScript program found on the explanation page of [Ver21], which can be referred to to reproduce the latex figures. This program is a starting point for further computations. Future work would be to investigate fractals produced from other hinged tilings, or with other related replacement rules.

REFERENCES

- [Bad13] Michael Bader. *Space-filling curves*, volume 9 of *Texts in Computational Science and Engineering*. Springer, Heidelberg, 2013. An introduction with applications in scientific computing.
- [Bar92] Paulo Taborda Barreto. Lines meeting on a surface the “mars” paperfolding. In *Proc. 3rd Int. Meeting of Origami Science, Mathematics, and Education*, edited by Koryo Miura., pages 342–59. Shiga, Japan: Seian Univeristy of Art and Deisgn 1997., 1992.
- [Böh20] Christian Böhm. Space-filling curves for high-performance data mining. *CoRR*, abs/2008.01684, 2020.
- [Bro08] Cameron Browne. Truchet curves and surfaces. *Computers & Graphics*, 32(2):268–281, 2008.
- [Car18] Christopher Carlson. Multi-scale truchet patterns. In Eve Torrence, Bruce Torrence, Carlo Séquin, and Kristóf Fenyvesi, editors, *Proceedings of Bridges 2018: Mathematics, Art, Music, Architecture, Education, Culture*, pages 39–44, Phoenix, Arizona, 2018. Tessellations Publishing.
- [Edg08] Gerald Edgar. *Measure, topology, and fractal geometry*. Undergraduate Texts in Mathematics. Springer, New York, second edition, 2008.
- [Fre02] Greg N. Frederickson. *Hinged dissections*. Cambridge University Press, New York, 2002. Swinging & twisting.
- [Hil91] David Hilbert. Ueber die stetige Abbildung einer Linie auf ein Flächenstück. *Math. Ann.*, 38(3):459–460, 1891.
- [Kra11] R. Krawczyk. Truchet tilings revisited. In *Proceedings of ISAMA 2011*, pages pp 69–77, 2011.
- [Lan18] Robert J. Lang. *Twists, tilings, and tessellations*. CRC Press, Boca Raton, FL, 2018. Mathematical methods for geometric origami.
- [Lin68] Aristid Lindenmayer. Mathematical models for cellular interactions in development ii. simple and branching filaments with two-sided inputs. *Journal of Theoretical Biology*, 18(3):300–315, 1968.
- [Ozk21] Mustafa Ismail Ozkaraca. *An application of space filling curves to substitution tilings*. *PhD thesis*. Glasgow University, 2021.
- [Pea90] G. Peano. Sur une courbe, qui remplit toute une aire plane. *Math. Ann.*, 36(1):157–160, 1890.
- [Sag94] Hans Sagan. *Space-filling curves*. Universitext. Springer-Verlag, New York, 1994.
- [Smi87] Cyril Stanley Smith. The tiling patterns of sebastian truchet and the topology of structural hierarchy. *Leonardo*, 20(4):373–385, 1987. With a translation of Truchet’s text by Pauline Boucher.
- [Tab14] Sergei Tabachnikov. Dragon curves revisited. *Math. Intelligencer*, 36(1):13–17, 2014.

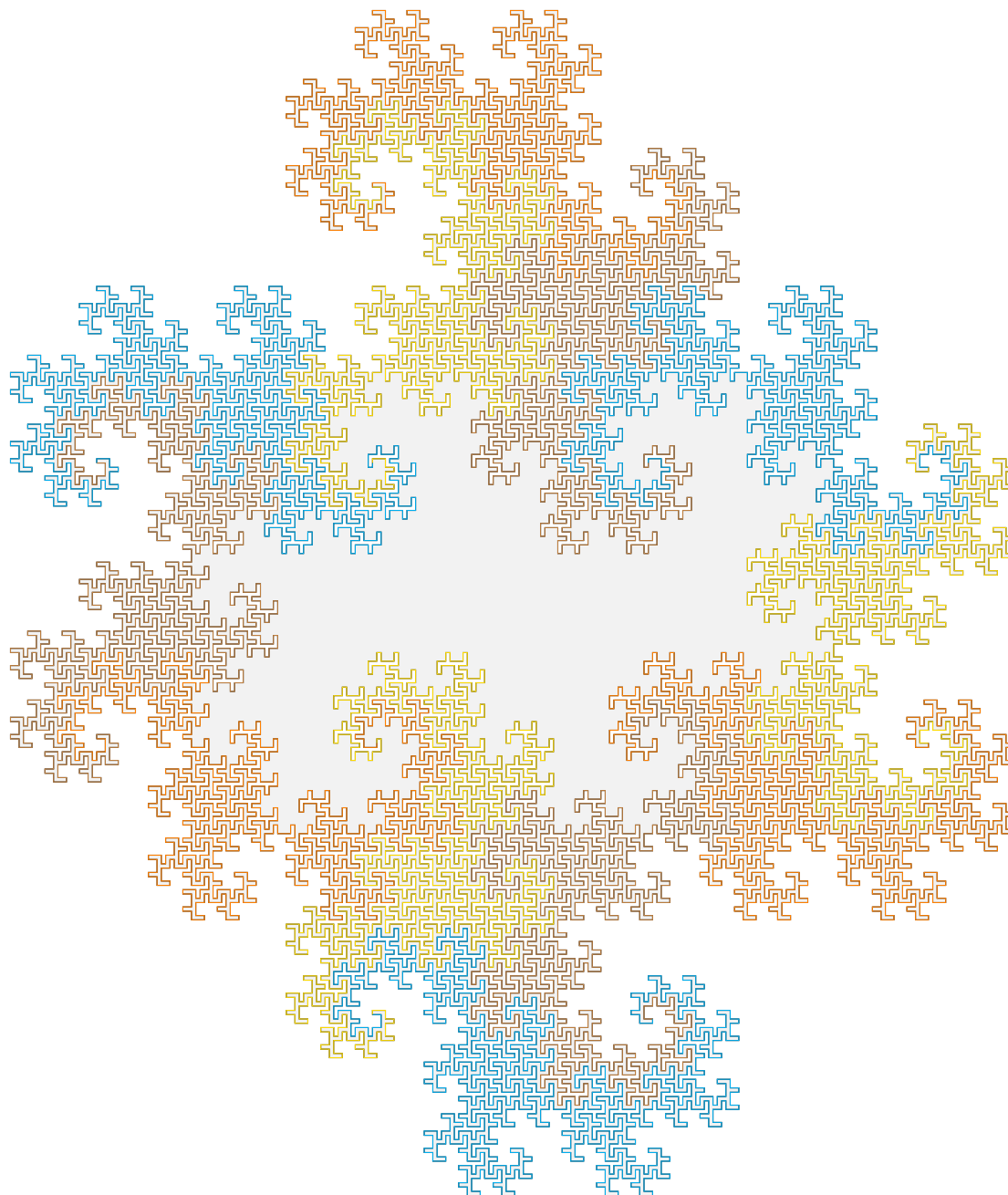


FIGURE 19. 0000000000 applied to $LLRLLRLLRLLR$ with diagonal line tile.

[Ver21] H. Verrill. Explanation, programs and generative art works. *web page*, 2021.
<https://www.mathamaze.co.uk/circles/trouchettree/fractaltrouchet.html>.

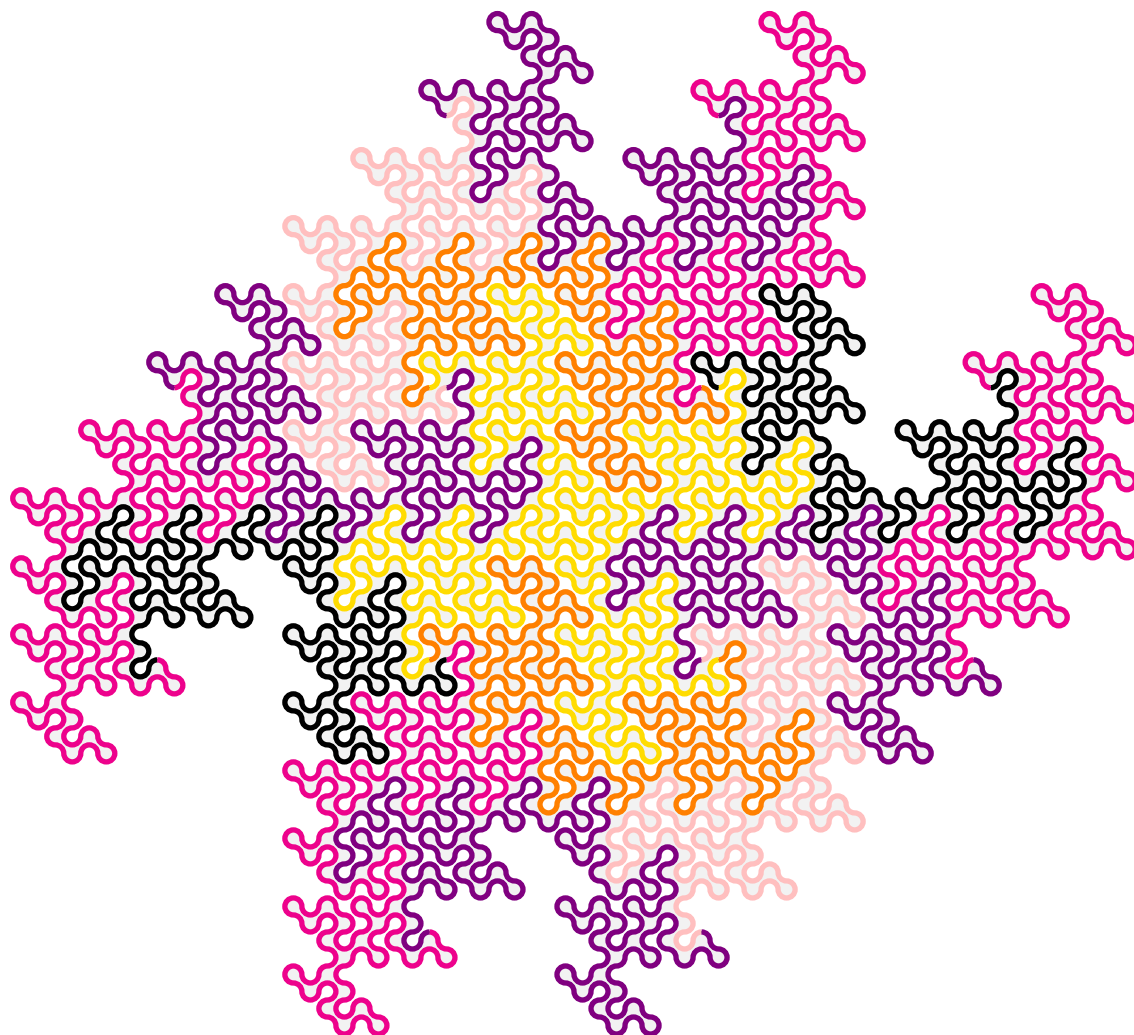


FIGURE 20. $00010001RLRRLRRRLLLRRRLR$ with quarter circles tile.



FIGURE 21. $(001)^3L$ with straight line tile.